25th ABCM International Congress of Mechanical Engineering
October 20-25, 2019, Uberlândia, MG, Brazil

COB-2019-1475
NUMERICAL STUDY OF THE HEAT TRANSFER RATE FOR UNSTEADY GÖRTLER VORTICES

Adriano Sueke Takata
Leandro Franco de Souza
Instituto de Ciências Matemática e Computação, Universidade de São Paulo, Campus São Carlos, Brasil
adrianostakata@gmail.com, lefraso@icmc.usp.br

Abstract. *The streamwise-oriented counter-rotating vortices also known as Görtler vortices occur due to the imbalance between centrifugal and inertial forces in boundary layer flows over concave walls. This kind of vortex appears in aerodynamic flow such as turbine blades and airfoils. Recently, the study in this area is focused on the evolution of vortices when unsteady disturbances are inserted. Some conclusions in these studies are that both spanwise wavelength and the frequency number has great importance in the behavior of the Görtler vortices. The change in the behavior of the vortices should influence the heat transfer rate due to the relationship between the velocity and thermal boundary layers. Thus, the present work aims to investigate the heat transfer rate using the Direct Numerical Simulation (DNS) when unsteady disturbances are inserted from blowing and suction of mass at the wall. The steady disturbances reached the highest heat transfer rates for the wavelength in the spanwise direction 9.0 and 18.0 mm. The point where the Görtler vortices begin to intensify the heat transfer rate is further away from the leading edge when is inserted unsteady disturbances. Moreover, the dominant mode has a greater influence on the heat transfer rate.*

Keywords: *Unsteady Görtler Vortices, Heat Transfer, Direct Numerical Simulation, Non-linear Analysis*

1. INTRODUCTION

The instability study of the Navier-Stokes equations has as objective to understand the laminar-turbulent transition process of a fluid flow. This work focuses on the instability in boundary layers over concave surfaces where due to the imbalance between the centrifugal and inertial forces may lead to the formation of streamwise-oriented counter-rotation vortices (Saric and William, 1994). These vortices were studied initially by Görtler (1941) which bears his name. The Görtler vortices have great importance in the aeronautical industry because they appear in several aerodynamic flows as turbine blades (Brown and Martin, 1981) and airfoils (Wang *et al.*, 2018).

The vortices are studied both experimentally and numerically inserting infinitesimal disturbances. There are several ways to introduce these perturbations such as surface roughness, acoustic vibrations, wall-transpiration, among other (for more details see Denier *et al.* (1991) and (Souza *et al.*, 2004)). Furthermore, the disturbances are classified herein as steady and unsteady.

Initially, the researchers considered only the steady disturbances and the system of equations was isothermal. Boiko *et al.* (2010) published the first experimental and numerical study about unsteady disturbances. Since then, several researchers have been studying this topic (Xu *et al.*, 2017), (Marensi and Ricco, 2017), (Boiko *et al.*, 2017), and (Borodulin *et al.*, 2018). The studies considering heat transfer are much older than unsteady disturbances, since we are always interested in reducing the energy consumption of the system. A review on this topic can be found in the following articles (Brown and Martin, 1981), (Fiebig, 1997), (Liu, 2008), and (Malatesta *et al.*, 2017).

The objective of the present work is to investigate the heat transfer rate through the Stanton number for two different spanwise wavelengths using the direct numerical simulation when the unsteady disturbances are inserted in the flow field.

2. MATHEMATICS FORMULATION

The governing equations used to model this phenomenon are the incompressible Navier-Stokes and heat transfer equations in the curvilinear system being x^* streamwise, y^* wall-normal and z^* spanwise coordinate with Lamé coefficients $h_1 = 1 - y^* k_c^*$ and $h_2 = h_3 = 1$ (Floryan *et al.*, 1982), where $k_c^* = 1/R^*$ is the wall curvature and R^* is the radius of curvature (the symbol $*$ mean dimensional variable). The variables are dimensionaless as follow:

$$x = \frac{x^*}{L^*}; \quad y = \frac{y^*}{L^*}; \quad z = \frac{z^*}{L^*}; \quad t = \frac{t^* U_\infty^*}{L^*}; \quad k_c = \frac{L^*}{R^*};$$

$$\tilde{u} = \frac{u^*}{U^*_\infty}; \quad \tilde{v} = \frac{v^*}{U^*_\infty}; \quad \tilde{w} = \frac{w^*}{U^*_\infty}; \quad \tilde{p} = \frac{p^*}{\rho U^{*2}_\infty}: \quad \tilde{\theta} = \frac{T^* - T^*_0}{T^*_\infty - T^*_0},$$

where the variables ($\tilde{u},\ \tilde{v},\ \tilde{w},\ \tilde{p},\ \tilde{T}$) are the velocities, pressure and temperature components, U^*_∞ is the freestream velocity, ρ is the density, T^∞_0 is the surface temperature and T^*_∞ is the freestream temperature. Furthermore, it is used order of magnitude analysis to eliminate curvature terms of higher order.

The methodologies utilized to simplify the governing equations are: (a) the vorticity -velocity formulation to eliminate the pressure terms; (b) the vorticity, velocity and temperature components are decomposed in baseflow and perturbation parts, in other words, a generic component $\tilde{\phi}$ is decomposed as:

$$\tilde{\phi}(x, y, z, t) = \phi_b(x, y, z) + \phi(x, y, z, t),$$

where ϕ_b and ϕ is the baseflow and perturbation parts. The baseflow part can be simplified into a two-dimensional problem because the freestream velocity is parallel and perpendicular to the x and y-axes, respectively. The perturbation part is given by follow the following system of equations:

$$\frac{\partial \omega_x}{\partial t} + \frac{\partial a}{\partial y} - \frac{\partial b}{\partial z} + \frac{Go^2}{\sqrt{Re}}\frac{\partial d}{\partial z} = \frac{1}{Re}\nabla^2\omega_x \tag{1}$$

$$\frac{\partial \omega_y}{\partial t} + \frac{\partial c}{\partial z} - \frac{\partial a}{\partial x} = \frac{1}{Re}\nabla^2\omega_y \tag{2}$$

$$\frac{\partial \omega_z}{\partial t} + \frac{\partial b}{\partial x} - \frac{\partial c}{\partial y} - \frac{Go^2}{\sqrt{Re}}\frac{\partial d}{\partial x} = \frac{1}{Re}\nabla^2\omega_z \tag{3}$$

$$\frac{\partial u}{\partial x} + \frac{\partial v}{\partial y} + \frac{\partial w}{\partial z} = 0 \tag{4}$$

$$\frac{\partial^2 u}{\partial x^2} + \frac{\partial^2 u}{\partial z^2} = -\frac{\partial \omega_y}{\partial z} - \frac{\partial^2 v}{\partial x \partial y} \tag{5}$$

$$\frac{\partial^2 v}{\partial x^2} + \frac{\partial^2 v}{\partial y^2} + \frac{\partial^2 v}{\partial z^2} = -\frac{\partial \omega_z}{\partial x} + \frac{\partial \omega_x}{\partial z} \tag{6}$$

$$\frac{\partial^2 w}{\partial x^2} + \frac{\partial^2 w}{\partial z^2} = +\frac{\partial \omega_y}{\partial x} - \frac{\partial^2 v}{\partial y \partial z} \tag{7}$$

$$\frac{\partial \theta}{\partial t} + \frac{\partial e}{\partial x} + \frac{\partial f}{\partial y} + \frac{\partial g}{\partial z} = \frac{1}{Re\ Pr}\nabla^2\theta, \tag{8}$$

where the variables ($u,\ v,\ w,\ \omega_x,\ \omega_y,\ \omega_z,\ \theta$) are the disturbance velocity, vorticity and temperature component. The Reynolds, Görtler and Prandtl numbers are defined as $Re = U^*_\infty L^*/\nu^*$, $Go = (k^*_c\sqrt{Re})^{1/2}$ and $Pr = \nu^*/\alpha^*$ respectively, where U^*_∞ is freestrem velocity, ν is kinematic viscosity and α^* is the thermal diffusivity of the fluid. In addition, the other variables are defined as (when a bar on top of the variables implies baseflow quantities):

$$a = \omega_x(v_b + v) - \omega_y(u_b + u); \quad b = \omega_z u + \omega_z u_b + \bar{\omega}_z u - \omega_x w; \quad c = \omega_y w - \omega_{zb} v - \omega_z v_b - \omega_z v;$$

$$d = 2u_b u + u^2; \quad e = u_b\theta + u\theta_b + u\theta; \quad f = v_b\theta + v\theta_b + v\theta; \quad and \quad g = w(\theta_b + \theta).$$

The boundary conditions used for the system of equations of the base and perturbed flow are similar to those of the articles (Kloker *et al.*, 1993) and (Malatesta *et al.*, 2017). The exception is the disturbance insertion region that is described better in the next section.

3. NUMERICAL FORMULATION

Experiments related to Görtler vortices indicate that in the spanwise direction the flow is periodic (Swearingen and Blackwelder, 1987). Thus, the components are represented are represented by the linear combination of $K + 1$ Fourier modes, in other words, it has:

$$\phi(x, y, z, t) = \sum_{k=0}^{K} \Phi_k(x, y, t) e^{-i\beta_k z}, \tag{9}$$

where ϕ is some property of the flow, $i = \sqrt{-1}$ the imaginary unit, k denote the Fourier modes and $\beta_k = 2\pi k L^*/\lambda_z^*$ is the spanwise wavenumber and λ_z^* is the spanwise wavelength.

Replacing the expression (9) for all components of the equations (1)-(8) obtains the following system of equations for $k = 0, \ldots, K$.

$$\frac{\partial \Omega_{xk}}{\partial t} + \frac{\partial A_k}{\partial y} + i\beta_k B_k - i\beta_k \frac{Go^2}{\sqrt{Re}} D_k = \frac{1}{Re}\nabla_k^2 \Omega_{xk}, \tag{10}$$

$$\frac{\partial \Omega_{yk}}{\partial t} - i\beta_k C_k - \frac{\partial A_k}{\partial x} = \frac{1}{Re}\nabla_k^2 \Omega_{yk}, \tag{11}$$

$$\frac{\partial \Omega_{zk}}{\Omega t} + \frac{\partial B_k}{\partial x} - \frac{\partial C_k}{\partial y} - \frac{Go^2}{\sqrt{Re}} \frac{\partial D_k}{\partial x} = \frac{1}{Re}\nabla_k^2 \Omega_{zk}, \tag{12}$$

$$\frac{\partial U_k}{\partial x} + \frac{\partial V_k}{\partial y} - i\beta_z W_k = 0, \tag{13}$$

$$\frac{\partial^2 U_k}{\partial x^2} - \beta_k^2 U_k = i\beta_k \Omega_{yk} - \frac{\partial^2 V_k}{\partial x \partial y}, \tag{14}$$

$$\frac{\partial^2 V_k}{\partial x^2} + \frac{\partial^2 V_k}{\partial y^2} - \beta_k^2 V_k = -\frac{\partial \Omega_{yk}}{\partial x} - i\beta_k \Omega_{xk}, \tag{15}$$

$$\frac{\partial^2 W_k}{\partial x^2} - \beta_k^2 W_k = \frac{\partial \Omega_{yk}}{\partial x} + i\beta_k \frac{\partial V_k}{\partial y}, \tag{16}$$

$$\frac{\partial \Theta_k}{\partial t} + \frac{\partial E_k}{\partial x} + \frac{\partial F_k}{\partial y} - i\beta_k G_k = \frac{1}{Re\ Pr}\nabla^2 \Theta_k, \tag{17}$$

where

$$\nabla_k^2 = \left(\frac{\partial^2}{\partial x^2} + \frac{\partial^2}{\partial y^2} - \beta_k^2 \right).$$

The computational domain is illustrated in the Fig. 1, where the inflow is at $x = x_0$, the damping region is at $x_1 \leq x \leq x_2$, the disturbance is introduced at $x_2 \leq x \leq x_3$, the region of interest is localized at $x_3 \leq x \leq x_4$, the relaminarization rgion is at $x_4 \leq x \leq x_5$, and the outflow is at $x = x_{\max}$.

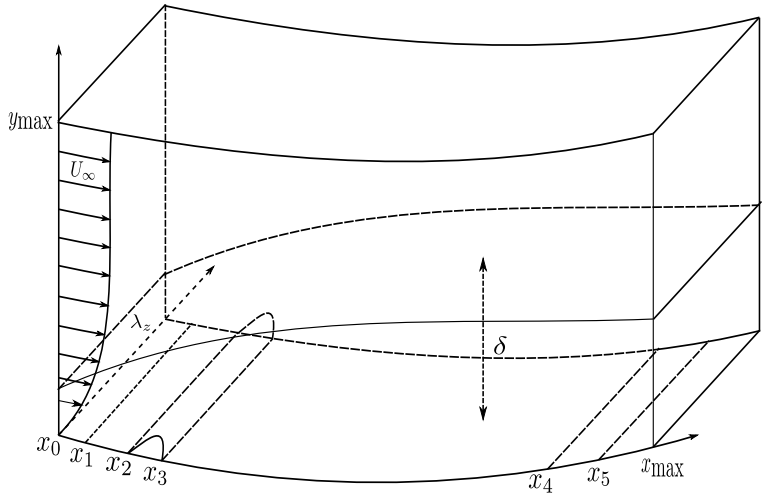

Figure 1. Computational domain, where the inflow is at $x = x_0$, the damping region is at $x_1 \leq x \leq x_2$, the disturbances are introduced at $x_2 \leq x \leq x_3$, the relaminarization region is at $x_4 \leq x \leq x_5$, and the outflow is the $x = x_{\max}$..

The disturbances are inserted through the suction and blowing of mass at the wall in the V_k velocity along the streamwise direction with $k = 1$. Thus, this boundary condition is given by:

$$V_1(x, 0, t) = \begin{cases} A\sin^3(\epsilon)\cos(\omega_{gv} t) & \text{for} \quad x \in [x_2, x_3] \\ 0 & \text{for} \quad x \in [x_0, x_2) \cup (x_3, x_{max}] \end{cases}, \tag{18}$$

where A is the amplitude, $\epsilon = \pi(x - x_2)/(x_3 - x_2)$, $\omega = 2\pi f^*_{gv} L/U^*_\infty$ and f^*_{gv} is the frequency.

The code used for the simulation is the High Order Parallel Code (HOPe). The temporal and spatial derivatives are approximated by classical 4th order Runge-Kutta integration (Ferziger and Peric, 2012) and the high order compact finite difference-schemes (Lele, 1992), respectively. The code is parallelized using the domain decomposition technique in the streamwise direction, and the MPI library makes the communication between them. Furthermore, in the wall-normal direction is used the stretching of the mesh. The validation and verification of the code can be found in the articles (Souza, 2017), (Malatesta *et al.*, 2017) and (Takata *et al.*, 2018).

4. RESULTS

The parameters adopted in the simulations are the same as the Swearingen and Blackwelder (1987), this is, the radius curvature is $R^* = 3.2\ m$, and the freestream velocity is $U^*_\infty = 5.0\ m/s$. The kinematic viscosity considered is $\nu^* = 1.509 \times 10^{-5}\ m^2/s$, the thermal diffusivity of the fluid is $\alpha^* = 2.095 \times 10^{-5}\ m^2/s$ and reference length used is $L^* = 0.1\ m$. Thus, the following values for the Reynolds, Görtler and Prandtl numbers are $Re = 33124.0$, $Go = 2.385$ and $Pr = 0.72$ respectively. The spanwise wavelength considered are $\lambda^*_z = 9.0$ e $18.0\ mm$ with respective values for the wavelength of the fundamental Fourier mode $\Lambda = 158.099$ e 447.173.

The distance between two consecutive points at streamwise direction is $dx = 2.0 \times 10^{-2}$ and the initial spacing at wall-normal direction is $dy = 5.0 \times 10^{-4}$ with stretching of 1%. The temporal step is $dt = 1.0 \times 10^{-3}$. In the spanwise direction is adopted 21 Fourier modes and it is considered 64 points in the physical space. The disturbances are introduced between at $x_2 = 1.2$ and $x_3 = 1.52$. The maximum amplitude used is $A = 3.5 \times 10^{-3}$ e 1.08×10^{-3}, for $\lambda^*_z = 9.0$, e $18.0\ mm$ respectively. Furthermore, it is considered five frequencies $f^*_{gv} = 3, 6, 9, 12$, and $15\ Hz$ with their respective dimensionless values $\omega_{gv} = 0.3769,\ 0.7539,\ 1.1309, 1.5079$, and 1.8849.

The influence of the Görtler vortices generated by the unsteady disturbances is analyzed through the rate of heat transfer calculated by the mean of the local Stanton number in the spanwise direction and in time. The Stanton number is defined:

$$St_x = \frac{Nu_x}{PrRe_x}, \quad \text{with} \quad Nu_x = \left.\frac{\partial T}{\partial y}\right|_{\text{wall}} \frac{x^*}{T^*_\infty - T^*_0},$$

where Nu_x is the local Nusselt number. The performance of the rate of heat transfer obtained in the simulation is compared using the mean curves of the Stanton number of the laminar and turbulent flow extracted from (Bergman *et al.*, 2011). They are defined by:

$$St_{lam} = 0.332 Re_x^{-1/2} Pr^{-2/3} \quad \text{and} \quad St_{tur} = 0.0296 Re_x^{-1/5} Pr^{-2/3}.$$

In the $\lambda^*_z = 9.0$ mm case, it is used Nx=825 and Ny=297 points for all the frequencies. In Fig. 2, it is presented the evolution in the streamwise direction of the mean local Stanton number in the spanwise and in time, which observes the decreases of the heat transfer rate when the frequency increases. According to the article of Takata *et al.* (2018), the dominant mode in all cases is $(1, 1)$, that is, only a pair of Gortler vortices are generated and their direction of rotation changes with each half cycle of the $\cos(\omega_{gv} t)$ function. Moreover, the point where Görtler vortices begin to intensify the heat transfer rate is further away from the leading edge as the frequency increases. Note also that there is no difference in the heat transfer rate between laminar and $f^*_{gv} = 15\ Hz$ cases.

The Tab. 1 shows the percentage of the heat transfer rate between the laminar and transient flows and between the transient and turbulent flows for $\lambda_z = 9.0\ mm$ and for all frequencies case at the point $x = 15.0$.

Table 1. The heat transfer rate in percentage between the laminar and transitional flows and between the transient and turbulent flows at the point $x = 15.0$.

f_{gv}	St_x	laminar-transitional	transitional-turbulent
0	2.1693×10^{-3}	269.99%	16.32%
3	1.8760×10^{-3}	219.97%	27.63%
6	1.5726×10^{-3}	168.22%	39.34%
9	1.0902×10^{-3}	85.94%	57.95%
12	6.1860×10^{-4}	5.50%	76.14%
15	5.8336×10^{-4}	0.12%	77.49%

In the $\lambda^*_z = 18.0\ mm$ case, it is used Nx $= 905$ and Ny $= 297$ points for all the frequencies. In Fig. 3, it is presented the results of the evolution in the streamwise direction of the mean local Stanton number in the spanwise and in time, which one can observe two behaviours. The first behavior is the same as $\lambda_z = 9.0\ mm$ case and happens for $f_{gv} = 3$ and $6\ Hz$. The second behavior is that the heat transfer rate is close to the case where the disturbance is steady and happens

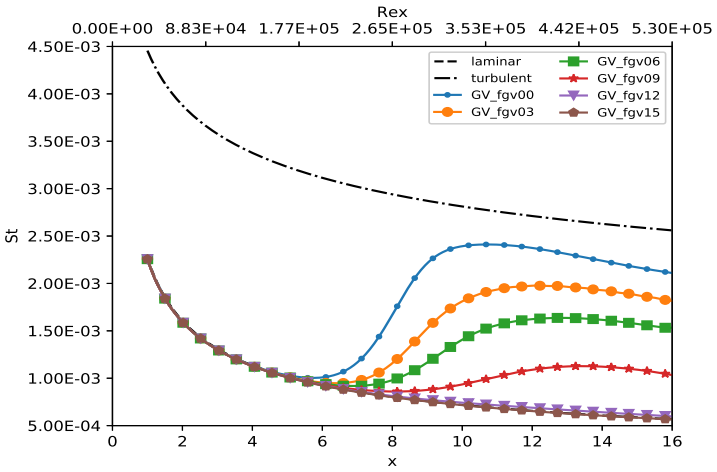

Figure 2. The evolution in the streamwise direction of the mean local Stanton number in the spanwise direction and in time for $\lambda_z^* = 9.0\ mm$.

for $f_{gv} = 9, 12$, and $15\ Hz$. The dominant mode can explain those two distinct behaviors. According to the studies of Takata *et al.* (2018), for $f_{gv} = 3$ and $6\ Hz$ cases, the dominant mode is $(1, 1)$ and, so its behavior is similar to the $\lambda_z = 9.0\ mmm$ case, whereas, for $f_{gv} = 9, 12$, and $15\ Hz$, the dominant mode is $(0, 2)$, this is, a stationary mode which generates two pairs of Görtler vortices that dominate the flow. Moreover, the behavior of the point where the Görtler vortices begin to intensify the heat transfer rate is opposite of the dominant mode $(1, 1)$, this is, the point gets closer to the leading edge as the frequency increases. Note also that there is an oscillation of high frequency in the graphics of $f_{gv} = 3$ and $6\ Hz$. This oscillation is due to secondary instability that is naturally generated by high-frequency modes. Unfortunately, in the present work will not be explored this phenomenon.

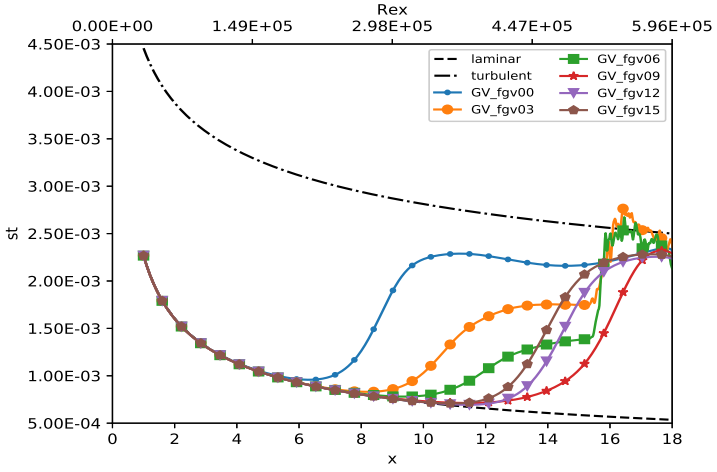

Figure 3. The evolution in the streamwise direction of the mean local Stanton number in the spanwise direction and in time for $\lambda_z^* = 18.0\ mm$.

The Tab. 2 shows the percentage of the heat transfer rate bewteen the laminar and transient flows and bewteen the transient and turbulent flows for $\lambda_z = 18.0\ mm$ and for $f_{gv} = 0,\ 3$, and $6\ Hz$ at the point $x = 15.0$ and in the Tab. 3, it is presented the results for $f_{gv} = 0,\ 9,\ 12$, and $15\ Hz$. at the point $x = 17.5$.

Table 2. The heat transfer rate in percentage between the laminar and transitional flows and between the transient and turbulent flows for $f_{gv} = 0,\ 3$ e $6\ Hz$ at the point $x = 15.0$.

f_{gv}	St_x	laminar-transitional	transitional-turbulent
0	2.1643×10^{-3}	269.14%	16.51%
3	1.7507×10^{-3}	198.59%	32.47%
6	1.3784×10^{-3}	135.11%	46.83%

Table 3. The heat transfer rate in percentage between the laminar and transitional flows and between the transient and turbulent flows for $f_{gv} = 0,\ 9,\ 12$ and $15\ Hz$ at the point $x = 17.5$.

f_{gv}	St_x	laminar-transitional	transitional-turbulent
0	2.3344×10^{-3}	330.061%	7.13%
9	2.3138×10^{-3}	326.26%	7.95%
12	2.2556×10^{-3}	315.53%	10.27%
15	2.2805×10^{-3}	320.12%	9.28%

5. CONCLUSION

In the present work, the heat transfer rate for unsteady Gortler vortices was analyzed using numerical simulation. The cases were for the wavelengths in the spanwise direction $\lambda_z = 9.0$ and $18.0\ mm$, which were inserted disturbances as the frequencies $f_{gv} = 0,\ 3,\ 6,\ 9,\ 12$, and $15\ Hz$. For both the cases $\lambda_z = 9.0$ and $18.0\ mm$ the steady disturbances ($f_{gv} = 0\ Hz$) was that obtained the highest heat transfer rate. For the unsteady disturbances, the point where the Görtler vortices begin to intensify the heat transfer rate is further away from the leading edge regarding the steady disturbance. Furthermore, the dominant mode has a great influence on the heat transfer rate.

6. ACKNOWLEDGEMENTS

We thank CAPES and FAPESP for financial support and ICMC-USP for technical support and infrastructure. Research carried out using the computational resource of the Center for Mathematical Applied to Industry (CeMEAI) funded by FAPESP (Process Number 2013/07375-0).

7. REFERENCES

Bergman, T.L., Incropera, F.P., DeWitt, D.P. and Lavine, A.S., 2011. *Fundamentals of heat and mass transfer*. John Wiley & Sons.

Boiko, A.V., Ivanov, A.V., Kachanov, Y.S. and Mischenko, D.A., 2010. "Steady and unsteady görtler boundary-layer instability on concave wall". *European Journal of Mechanics-B/Fluids*, Vol. 29, No. 2, pp. 61–83.

Boiko, A.V., Ivanov, A.V., Kachanov, Y.S., Mischenko, D.A. and Nechepurenko, Y.M., 2017. "Excitation of unsteady görtler vortices by localized surface nonuniformities". *Theoretical and Computational Fluid Dynamics*, Vol. 31, No. 1, pp. 67–88.

Borodulin, V.I., Ivanov, A.V., Kachanov, Y.S. and Mischenko, D.A., 2018. "Systematic study of distributed excitation of unsteady görtler modes by freestream vortices". *European Journal of Mechanics-B/Fluids*, Vol. 68, pp. 167–183.

Brown, A. and Martin, B.W., 1981. "Flow transition phenomena and heat transfer over the pressure surfaces of gas turbine blades". In *ASME 1981 International Gas Turbine Conference and Products Show*. American Society of Mechanical Engineers, pp. V003T09A013–V003T09A013.

Denier, J.P., Hall, P. and Seddougui, S.O., 1991. "On the receptivity problem for görtler vortices: vortex motions induced by wall roughness". *Phil. Trans. R. Soc. Lond. A*, Vol. 335, No. 1636, pp. 51–85.

Ferziger, J.H. and Peric, M., 2012. *Computational methods for fluid dynamics*. Springer Science & Business Media.

Fiebig, M., 1997. "Vortices and heat transfer". *ZAMM-Journal of Applied Mathematics and Mechanics/Zeitschrift für Angewandte Mathematik und Mechanik*, Vol. 77, No. 1, pp. 3–18.

Floryan, J.M., Saric and William, S., 1982. "Stability of gortler vortices in boundary layers". *AIAA journal*, Vol. 20, No. 3, pp. 316–324.

Görtler, H., 1941. "Instabilität laminarer grenzschichten an konkaven wänden gegenüber gewissen dreidimensionalen störungen". *ZAMM - Journal of Applied Mathematics and Mechanics / Zeitschrift für Angewandte Mathematik und Mechanik*, Vol. 21, No. 4, pp. 250–252.

Kloker, M., Konzelmann, U. and Fasel, H., 1993. "Outflow boundary conditions for spatial navier-stokes simulations oftransition boundary layers". *AIAA journal*, Vol. 31, No. 4, pp. 620–628.

Lele, S.K., 1992. "Compact finite difference schemes with spectral-like resolution". *Journal of computational physics*, Vol. 103, No. 1, pp. 16–42.

Liu, J.T.C., 2008. "Nonlinear instability of developing streamwise vortices with applications to boundary layer heat transfer intensification through an extended reynolds analogy". *Philosophical Transactions of the Royal Society A: Mathematical Physical and Engineering Sciences*, Vol. 366.

Malatesta, V., Rogenski, J.K. and Souza, L.F., 2017. "Heat transfer enhancement via görtler flow with spatial numerical simulation". *International Journal of Numerical Methods for Heat & Fluid Flow*, Vol. 27, No. 1, pp. 189–209.

Marensi, E. and Ricco, P., 2017. "Growth and wall-transpiration control of nonlinear unsteady görtler vortices forced by

free-stream vortical disturbances". *Physics of Fluids*, Vol. 29, No. 11, p. 114106.

Saric and William, S., 1994. "Görtler vortices". *Annual Review of Fluid Mechanics*, Vol. 26, No. 1, pp. 379–409.

Souza, L.F., 2017. "On the odd and even secondary instabilities of görtler vortices". *Theoretical and Computational Fluid Dynamics*, Vol. 31, No. 4, pp. 405–425.

Souza, L.F., Mendonça, M.T., Medeiros, M.A.F. and Kloker, M., 2004. "Seeding of görtler vortices through a suction and blowing strip". *Journal of the Brazilian Society of Mechanical Sciences and Engineering*, Vol. 26, No. 3, pp. 269–279.

Swearingen, J.D. and Blackwelder, R.F., 1987. "The growth and breakdown of streamwise vortices in the presence of a wall". *Journal of Fluid Mechanics*, Vol. 182, pp. 255–290.

Takata, A.S., Rogenski, J.K. and Souza, L.F., 2018. "Numerical study of the influence of spanwise wavelength on the evolution of görtler vortices for unsteady disturbances". In *Brazilian Congress of Thermal Sciences and Engineering - ENCIT*. ABCM.

Wang, J.S., Feng, L.H., Wang, J.J. and Li, T., 2018. "Görtler vortices in low-reynolds-number flow over multi-element airfoil". *Journal of Fluid Mechanics*, Vol. 835, pp. 898–935.

Xu, D., Zhang, Y. and Wu, X., 2017. "Nonlinear evolution and secondary instability of steady and unsteady görtler vortices induced by free-stream vortical disturbances". *Journal of Fluid Mechanics*, Vol. 829, pp. 681–730.

8. RESPONSIBILITY NOTICE

The authors are the only responsible for the printed material included in this paper.